Research Article | Vol. 25, No. 3 | 6 Feb 2017 | OPTICS EXPRESS 2153

Optics EXPRESS

Angle-tolerant linear variable color filter based on a tapered etalon

PENG JI,[1] CHUL-SOON PARK,[1] SONG GAO,[1] SANG-SHIN LEE,[1,*] AND DUK-YONG CHOI[2]

[1]*Department of Electronic Engineering, Kwangwoon University, 20 Kwangwoon-ro, Nowon-gu, Seoul 01897, South Korea*
[2]*Laser Physics Centre, Research School of Physics and Engineering, Australian National University, Canberra ACT 2601, Australia*
[*]*slee@kw.ac.kr*

Abstract: We propose and fabricate a linear variable color filter (LVCF) that possesses an enhanced angular tolerance in conjunction with a wide linear filtering range (LFR) by taking advantage of an Ag-TiO_2-Ag configuration. The TiO_2 cavity is tapered in thickness along the device so that the resonance wavelength can be continuously tuned according to the position. In addition, the metal-dielectric-metal structure is overlaid with a pre-designed graded anti-reflection coating in SiO_2 to complete the etalon, thereby maximizing the transmission efficiency across the entire device. The tapered dielectric layers in the proposed filter were fabricated via glancing angle deposition without the help of any mask or moving parts. The center wavelength was scanned from 410 nm to 566 nm, resulting in an LFR of 156 nm, and the overall spectra exhibited an approximate peak transmission of 40% and spectral bandwidth of 68 nm. The angular tolerance was as large as 45°, incurring a fractional wavelength shift below 4.2%. The resonance wavelength was verified to be linearly dependent on the position, providing a linearity beyond 99%. The proposed LVCF will thus be actively utilized in a portable micro-spectrometer and spectral scanning device.

OCIS codes: (230.7408) Wavelength filtering devices; (310.1210) Antireflection coatings; (310.4165) Multilayer design; (310.6860) Thin films, optical properties; (050.2230) Fabry-Perot; (050.5080) Phase shift.

References and links

1. R. R. McLeod and T. Honda, "Improving the spectral resolution of wedged etalons and linear variable filters with incidence angle," Opt. Lett. **30**(19), 2647–2649 (2005).
2. A. Emadi, H. Wu, S. Grabarnik, G. De Graaf, K. Hedsten, P. Enoksson, J. H. Correia, and R. F. Wolffenbuttel, "Fabrication and characterization of IC-compatible linear variable optical filters with application in a micro-spectrometer," Sens. Actuators A Phys. **162**(2), 400–405 (2010).
3. B. Sheng, P. Chen, C. Tao, R. Hong, Y. Huang, and D. Zhang, "Linear variable filters fabricated by ion beam etching with triangle-shaped mask and normal film coating technique," Chin. Opt. Lett. **13**(12), 122301 (2015).
4. L. Abel-Tibérini, F. Lemarquis, and M. Lequime, "Masking mechanisms applied to thin-film coatings for the manufacturing of linear variable filters for two-dimensional array detectors," Appl. Opt. **47**(30), 5706–5714 (2008).
5. A. Emadi, H. Wu, G. de Graaf, P. Enoksson, J. H. Correia, and R. Wolffenbuttel, "Linear variable optical filter-based ultraviolet microspectrometer," Appl. Opt. **51**(19), 4308–4315 (2012).
6. M. Ghaderi, N. P. Ayerden, A. Emadi, P. Enoksson, J. H. Correia, G. De Graaf, and R. F. Wolffenbuttel, "Design, fabrication and characterization of infrared LVOFs for measuring gas composition," J. Micromech. Microeng. **24**(8), 084001 (2014).
7. N. P. Ayerden, G. de Graaf, and R. F. Wolffenbuttel, "Compact gas cell integrated with a linear variable optical filter," Opt. Express **24**(3), 2981–3002 (2016).
8. X. Yu, Q. Lu, H. Gao, and H. Ding, "Development of a handheld spectrometer based on a linear variable filter and a complementary metal-oxide-semiconductor detector for measuring the internal quality of fruit," J. Near Infrared Spectrosc. **24**(1), 69–76 (2016).
9. A. Piegari and J. Bulir, "Variable narrowband transmission filters with a wide rejection band for spectrometry," Appl. Opt. **45**(16), 3768–3773 (2006).
10. A. Piegari, J. Bulir, and A. Krasilnikova Sytchkova, "Variable narrow-band transmission filters for spectrometry from space. 2. Fabrication process," Appl. Opt. **47**(13), C151–C156 (2008).

#283938 https://doi.org/10.1364/OE.25.002153
Journal © 2017 Received 2 Jan 2017; revised 18 Jan 2017; accepted 21 Jan 2017; published 25 Jan 2017
Corrected: 5 April 2017

Optics EXPRESS

11. L. Gao and L. V. Wang, "A review of snapshot multidimensional optical imaging: measuring photon tags in parallel," Phys. Rep. **616**, 1–37 (2016).
12. G. Shaw and H. Burke, "Spectral imaging for remote sensing," Linc. Lab. J. **14**(1), 3–28 (2003).
13. D. A. Boas, C. Pitris, and N. Ramanujam, *Handbook of Biomedical Optics* (Taylor and Francis, 2010), Chap. 7.
14. A. Gorman, D. W. Fletcher-Holmes, and A. R. Harvey, "Generalization of the Lyot filter and its application to snapshot spectral imaging," Opt. Express **18**(6), 5602–5608 (2010).
15. N. Hagan and M. W. Kudenov, "Review of snapshot spectral imaging technologies," Opt. Eng. **52**(9), 090901 (2013).
16. D. Dobbs, I. Gershkovich, and B. T. Cunningham, "Fabrication of a graded wavelength guided mode resonant filter photonic crystal," Appl. Phys. Lett. **89**(12), 123113 (2006).
17. H. A. Lin and C. S. Huang, "Linear variable filter based on a gradient grating period guided-mode resonance filter," IEEE Photonics Technol. Lett. **28**(9), 1042–1045 (2016).
18. L. Qian, D. Zhang, C. Tao, R. Hong, and S. Zhuang, "Tunable guided-mode resonant filter with wedged waveguide layer fabricated by masked ion beam etching," Opt. Lett. **41**(5), 982–985 (2016).
19. C. H. Ko, K. Y. Chang, and Y. M. Huang, "Analytical modeling and tolerance analysis of a linear variable filter for spectral order sorting," Opt. Express **23**(4), 5102–5116 (2015).
20. Delta Optical Thin Film A/S, "Continuously variable filters," http://www.deltaopticalthinfilm.com/products/linear-variable-filters.
21. Edmund Optics Inc, "Linear variable bandpass filters," http://www.edmundoptics.com/optics/optical-filters/bandpass-filters/linear-variable-bandpass-filters/3665.
22. H. Shin, M. F. Yanik, S. Fan, R. Zia, and M. Brongersma, "Omnidirectional resonance in a metal-dielectric-metal geometry," Appl. Phys. Lett. **84**(22), 4421–4423 (2004).
23. T. H. Noh, Y. T. Yoon, S. S. Lee, D. Y. Choi, and S. C. Lim, "Highly angle-tolerant spectral filter based on an etalon resonator incorporating a high index cavity," J. Opt. Soc. Korea **16**(3), 299–304 (2012).
24. J. L. Zhang, W. D. Shen, P. Gu, Y. G. Zhang, H. T. Jiang, and X. Liu, "Omnidirectional narrow bandpass filter based on metal-dielectric thin films," Appl. Opt. **47**(33), 6285–6290 (2008).
25. A. Hosseini and Y. Massoud, "Optical range microcavities and filters using multiple dielectric layers in metal-insulator-metal structures," J. Opt. Soc. Am. A **24**(1), 221–224 (2007).
26. K. T. Lee, S. Seo, J. Y. Lee, and L. J. Guo, "Ultrathin metal-semiconductor-metal resonator for angle invariant visible band transmission filters," Appl. Phys. Lett. **104**(23), 231112 (2014).
27. Y. K. Wu, A. E. Hollowell, C. Zhang, and L. J. Guo, "Angle-insensitive structural colours based on metallic nanocavities and coloured pixels beyond the diffraction limit," Sci. Rep. **3**, 1194 (2013).
28. K. T. Lee, S. Seo, J. Y. Lee, and L. J. Guo, "Strong resonance effect in a lossy medium-based optical cavity for angle robust spectrum filters," Adv. Mater. **26**(36), 6324–6328 (2014).
29. M. Born and E. Wolf, *Principles of Optics*, 7th ed. (Cambridge University, 1999), Chaps. 7 and 14.
30. C. S. Park, V. R. Shrestha, S. S. Lee, E. S. Kim, and D. Y. Choi, "Omnidirectional color filters capitalizing on a nano-resonator of Ag-TiO_2-Ag integrated with a phase compensating dielectric overlay," Sci. Rep. **5**, 8467 (2015).
31. M. Ohring, *Materials Science of Thin Films*, 2nd ed. (Academic, 2001), Chap. 3.
32. T. H. Noh, Y. T. Yoon, S. S. Lee, D. Y. Choi, and S. C. Lim, "Highly angle-tolerant spectral filter based on an etalon resonator incorporating a high index cavity," J. Opt. Soc. Korea **16**(3), 299–304 (2012).
33. K. T. Lee, J. Y. Lee, S. Seo, and L. J. Guo, "Colored ultra-thin hybrid photovoltaics with high quantum efficiency," Light Sci. Appl. **3**(10), e215 (2014).
34. H. Kang, S. Jung, S. Jeong, G. Kim, and K. Lee, "Polymer-metal hybrid transparent electrodes for flexible electronics," Nat. Commun. **6**, 6503 (2015).
35. R. Jin, W. Chen, and T. W. Simpson, "Comparative studies of metamodelling techniques under multiple modelling criteria," Struct. Multidiscipl. Optim. **23**(1), 1–13 (2001).

1. Introduction

A linear variable filter (LVF) is perceived to be indispensable to embody micro-spectrometers [1–5], sensors [6–8], hyperspectral imaging systems [9–12], and spectral scanning systems [13–15] due to its high resolving power, CMOS-compatible fabrication process, compactness, and spectral tunability. So far, various types of LVFs have been developed including all-dielectric Fabry-Perot etalons relying on Bragg reflectors [2–8], metal-dielectric structures composed of a single metallic film sandwiched between dielectric stacks [9,10], and guided-mode resonance (GMR) based resonators [16–18]. In particular, sophisticated fabrication processes are required for the metal-dielectric stacks or GMR-based structures, which are not suitable for mass production [19]. All-dielectric etalons provide a high spectral resolution in conjunction with high transmission/reflection efficiencies, and such LVF devices are already commercially available from Delta and Edmund Optics [20,21]. However, reflecting mirrors comprised of a pair of Bragg reflectors can be created by stacking over 10 dielectric films [2–

Optics EXPRESS

8], with each layer requiring precise control in terms of its thickness. Recently, in light of its conspicuous role in realizing a spectrometer and a hyperspectral imaging system in the visible band, a linear variable color filter (LVCF) has been demonstrated based on a similar Bragg reflector-based etalon [2,3]. However, its spectral response was highly sensitive to the angle of incidence, and the linear filtering range (LFR) was relatively narrow due to a limitation in the free spectral range (FSR). A metal-dielectric-metal (MDM) configuration has been utilized to build a color filter, with an improved performance in the angular tolerance and filtering range [22–28].

In this paper, we propose and develop a transmission-type LVCF that incorporates an Ag-TiO_2-Ag structure and exhibits an improved angular tolerance, an enlarged LFR, and facile fabrication. The etalon resorts to a linearly tapered dielectric cavity in TiO_2 sandwiched between a pair of thin Ag films, and this structure is then overlaid with a similarly tapered SiO_2 film. The resonance can be continuously tuned by adjusting the tapered cavity along the device, and the tapered overlay serves as an anti-reflection coating (ARC) to locally maximize the transmission. The tapered structures were successfully produced via straightforward, low-cost fabrication based on glancing angle deposition. The prepared LVCF was principally evaluated in terms of the positional variations in the resonance wavelength, and the angular tolerance was checked by analyzing the phase relationship associated with the tapered etalon. The transmission, resonance wavelength, and phase shift were calculated using Essential Macleod (Version 9.8.436), a simulation tool based on the transfer matrix method.

2. Proposed LVCF capitalizing on a tapered etalon

The proposed transmission-type LVCF draws upon a tapered MDM of Ag-TiO_2-Ag etalon formed on a glass substrate, as depicted in Fig. 1. The dielectric cavity is composed of a tapered layer of TiO_2 that exhibits a low loss and a relatively high index in the visible band, and the metallic mirrors are based on Ag, which is rarely prone to an extinction induced by inter-band transitions, as shown in Appendix A. The proposed etalon is presumed to give rise to a linearly tunable filtering characteristic according to the position thereof, and the color output is principally related to the resonance wavelength, which can be locally tailored via the thickness of the cavity. The etalon is especially integrated with a tapered SiO_2 film, which functions as an ARC, thereby suppressing the reflection and preventing the Ag film from being oxidized. In response to the white light that impinges upon the LVCF, the transmission resonantly peaks when constructive interference transpires in the forward direction. The Fabry-Perot etalon with an MDM configuration is deemed to provide bandpass filtering characteristics, rendering a transmission of $T = (1-r)^2 / (1+r^2-2r\cos\delta)$. The transmission peaks for $\delta = \phi_{prop} - (\phi_a + \phi_b) = 2m\pi$, with m representing an integer and $\phi_{prop} = 4\pi n_2 d / \lambda$ standing for the propagation phase shift [29]. As a consequence, the cavity thickness can be determined by $d = \lambda(2m\pi + \phi_a + \phi_b) / 4\pi n_2$. Here, r is the reflection coefficient of the metal film, δ is the total phase shift that accumulates during a single round-trip within the dielectric cavity, ϕ_a and ϕ_b are the reflection phases at the top and bottom Ag-TiO_2 interfaces, respectively, λ is the resonance wavelength in vacuum, and n_2 is the refractive index of the dielectric cavity. For the ARC to boost the transmission, the thickness is determined by $t = \lambda / 4n_1$, where n_1 is the refractive index of the ARC [29,30]. Regarding both the cavity and the ARC, the thickness is supposed to be approximately linearly related to the resonance wavelength. To locally maximize the transmission for the LVCF, the ARC is designed to be adequately tapered in accordance with the position-dependent thickness of the cavity. The resonance wavelength is presumed to be continuously and linearly scanned in the visible band. In this respect, d is altered in a linear manner from 130 nm to 210 nm, and t is similarly varied from 71 nm to 98 nm.

Optics EXPRESS

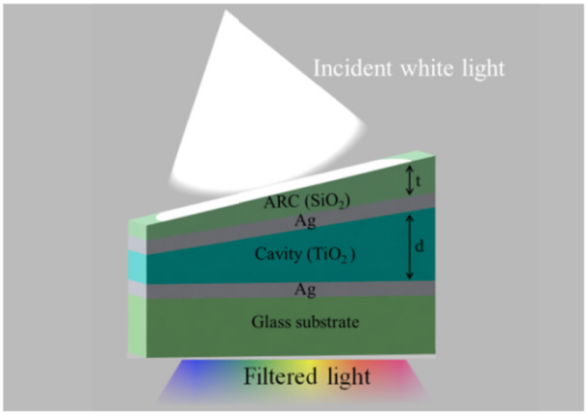

Fig. 1. Schematic configuration of the proposed transmissive LVCF resorting to a tapered etalon.

The proposed LVCF was characterized by assessing the spectral response depending on the position along it. As shown in Fig. 2, 9 different points of observation, including Pos. #0 through Pos. #8, were selected in such a way that the cavity thickness increases in increments of 10 nm. The thicknesses of the cavity and the ARC corresponding to the selected observation points are specifically listed in Fig. 2. Figure 3(a) plots the calculated spectral transmissions for different positions, providing approximately uniform transmission efficiencies and bandwidths. The resonance was observed to red-shift as the cavity thickness increases. The FSR, which determines the achievable LFR, was estimated to be about 173 nm for d = 210 nm, which is sufficient to cover the spectral band ranging from 398 nm to 571 nm. The LFR is defined by the two resonance wavelengths corresponding to Pos. #0 and Pos. #8. When the cavity thickness is tailored from 130 nm to 210 nm, the corresponding resonance wavelength ranges from 409 nm to 571 nm, resulting in an LFR of 162 nm. The designed filter presented a peak transmission of ~60% and a full-width-at-half-maximum bandwidth of ~35 nm on average. As plotted in Fig. 3(b), for each observation point on the LVCF, the resonance wavelength with respect to the thickness of the cavity and ARC was discovered to provide a good linear relationship. For a given LFR, the variation in thickness for the cavity is Δd = 80 nm, while that for the ARC is $\Delta t = \Delta d / 3 = \sim 27$ nm . The role played by the ARC was addressed in the case of the central position (Pos. #4), which assumes a cavity of d = 170 nm and an ARC of t = 85 nm. The dependence of the calculated transmission and reflection on the ARC is shown in Fig. 3(c). With the assistance of the designed ARC, the reflection was confirmed to have practically diminished from 13.3% to 2.8% and the transmission efficiency accordingly rises from 51.7% to 61.0%.

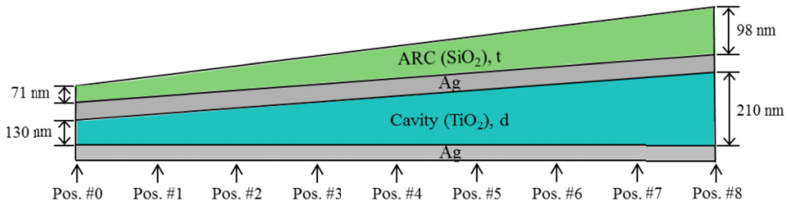

Position	#0	#1	#2	#3	#4	#5	#6	#7	#8
d (nm)	130	140	150	160	170	180	190	200	210
t (nm)	71	75	79	83	85	88	92	95	98

Fig. 2. Points of observation and the corresponding thicknesses of the cavity and ARC.

Optics EXPRESS

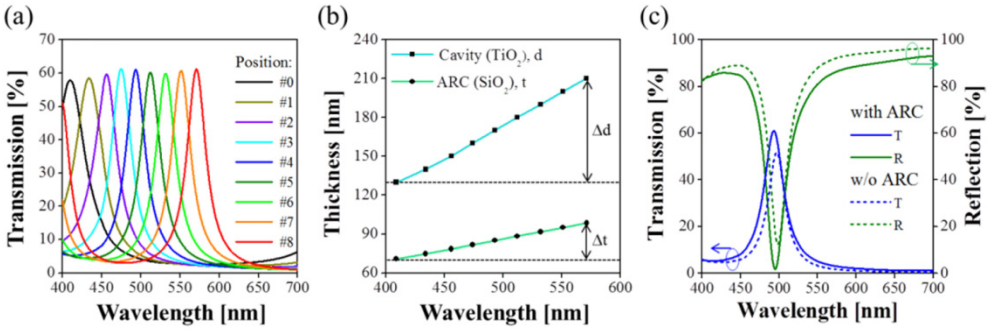

Fig. 3. (a) Calculated transmission with respect to the position. (b) Thicknesses of the cavity and ARC in terms of the resonance wavelength. (c) Transmission (T) and reflection (R) for the central position (Pos. #4) hinging on the presence of the ARC.

The influence of the incident angle on the transmission was then investigated for unpolarized light. Figure 4 shows the calculated transmission spectra in relation to the left-hand side (Pos. #1), center (Pos. #4), and right-hand side (Pos. #7) when the angle is varied from 0 to 45°. The angular tolerance is evaluated by referring to the shift in the center wavelength $\Delta\lambda$. The spectral shifts for Pos. #1, Pos. #4, and Pos. #7 were $\Delta\lambda$ = 15.6 nm, 16.1 nm, and 20.6 nm for an angle of 45°, respectively, which translates into fractional spectral shifts of $\Delta\lambda/\lambda$ = 3.6%, 3.2%, and 3.7%. The LVCF was revealed to give rise to a transmission peak that is nearly preserved at λ = 433 nm, 493 nm, and 551 nm regardless of the incident angle. Overall, the transmission declines by less than 7% for all the positions of interest. Then, with the intention to expound an angular tolerance of the proposed filter, the total phase shift was explored for the light that travels in the cavity. Considering that it taps into a tapered cavity and ARC, the LVCF can be modelled to mimic a flat multi-layer structure at a certain position, as described in Fig. 5(a). The total phase shift that accumulates during a single round-trip within the cavity is given by $\delta = 4\pi n_2 d(\cos\theta_p)/\lambda - (\phi_a + \phi_b)$ under oblique incidence, where θ_p represents the angle of propagation [30]. It is remarked that θ_p is equal to about 18° for n_2 = 2.26 and an incident angle of θ_i = 45° according to the Snell's law. As mentioned above, the transmission is maximized when the total phase shift satisfies $\delta = 2m\pi$. As shown in Figs. 5(b) through 5(d), the reflection phases of ϕ_a and ϕ_b are invariant to the different angles. The total phase shift that results from the propagation phase for the round-trip as well as the reflection phases at the top and bottom metal-dielectric interfaces nearly remains at 2π for the three positions mentioned above. Consequently, the resonance wavelength could remain stable in spite of the incident angle varying up to 45°.

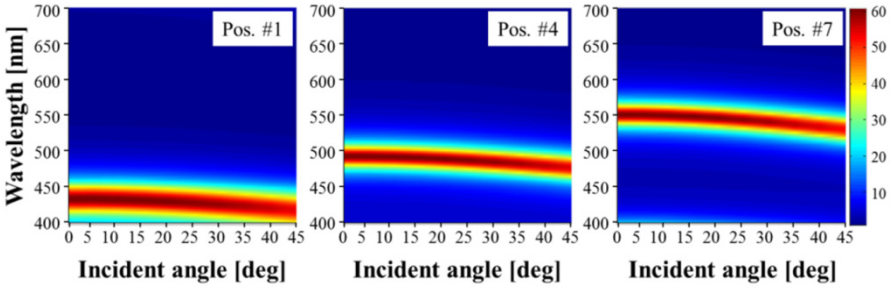

Fig. 4. Calculated transmission spectra in terms of the incident angle for three different positions.

Optics EXPRESS

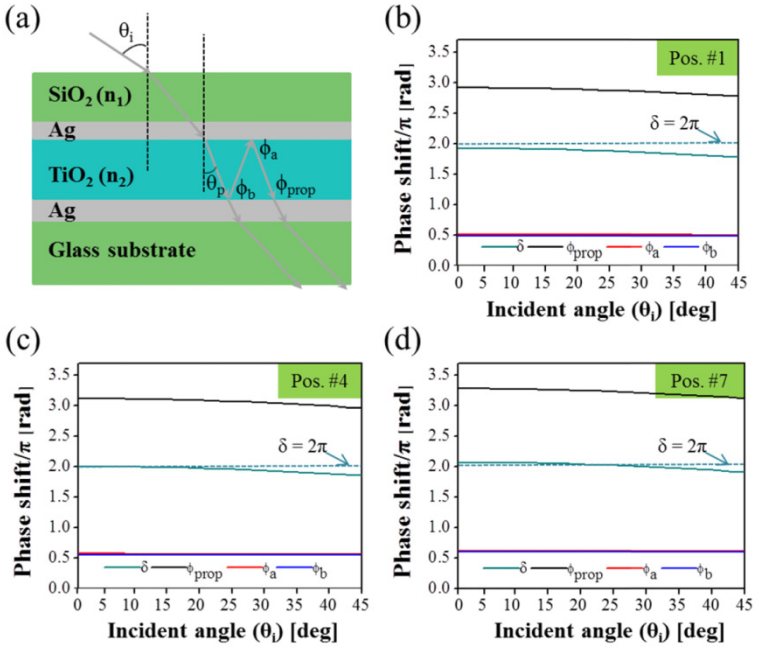

Fig. 5. (a) Modeling the propagation of light for the proposed LVCF. (b–d) Phase shift in response to a single round-trip, which is accounted for by the propagation phase and reflection phases at the top and bottom Ag-TiO_2 interfaces for the different positions of Pos. #1, #4, and #7.

3. Fabrication of the proposed LVCF and its experimental results

The proposed LVCF with an Ag-TiO_2-Ag-SiO_2 configuration was manufactured via e-beam evaporation (HVC-1200DA, Hanil Vacuum, S. Korea). To embody the tapered structure where the deposited film varies linearly in thickness, glancing angle deposition was introduced, as illustrated in Fig. 6(a). When the distance z_i between the material source and the position of the deposition on the substrate is within the mean-free-path of vapor, the deposition rate Λ pertaining to the evaporated material is given by $\Lambda \sim \cos\beta \cdot \cos^m(\alpha_i)/z_i^2$. Here α_i and β describe the divergence angle of the source and the angular slope of the tapered holder, respectively, and m is an integer that determines the geometry of the lobe-shaped vapor cloud and the angular distribution of the evaporation flux from the source [31]. As observed in Fig. 6(b), for both the cavity and the ARC, the thickness calculated in accordance with L exhibits a gradient, indicating that the thickness profile of the deposited layers can be tailored by adjusting the slope of the tapered holder β. During fabrication, the minimum distance z_0 was set to 50 cm. The deposition was performed at a temperature of 50 °C under a base pressure of 2×10^{-5} Torr, and the mean-free-path (250 cm) was assumed to be much larger than z_i, so that the evaporated particles could mostly go straight toward the substrate without experiencing collisions. Providing that the distance z_i is much larger than the size of the substrate L, the demonstrated rate of deposition is expected to vary almost linearly along the substrate.

The detailed fabrication procedure is illustrated in Fig. 7(a). An Ag film with a thickness of 30 nm, which acts as one of the metallic mirrors, was first deposited on a glass substrate via e-beam evaporation. A tapered TiO_2 cavity was subsequently created by exploiting a wedge-shaped holder with an angle of $\beta_1 = 60°$, according to the concept described in Fig. 6(a). With the tapered holder appended to the bottom of the substrate, the top thereof slants accordingly with the source target of TiO_2. As a result, the deposited dielectric cavity was

Optics EXPRESS

linearly tapered in accordance with the continuously varying distance between the source and the surface of the substrate. After removing the holder, the second Ag film was similarly built on top of the cavity so as to make the other mirror. Finally, a tapered SiO_2 coating was produced by taking advantage of a wedge-shaped holder with a taper of $\beta_2 = 30°$, in a similar manner to that of the cavity. The LVCF was completed with an effective area of 150 mm × 25 mm, for which the positional variation of the cavity thickness was estimated to be ~0.53 nm/mm. The color image available from the prepared filter is displayed in Fig. 7(b), wherein the observation points are individually marked. In response to the white light that is illuminated from the back of the LVCF, the transmitted optical output pertaining to the positions of Pos. #0 through Pos. #8 was monitored to yield a continuously varying vivid color that spans dark violet, blue, green, and yellow. The corresponding center wavelength ranged from 410 nm to 566 nm, providing a positional rate of the spectral shift that is equivalent to 1.04 nm/mm.

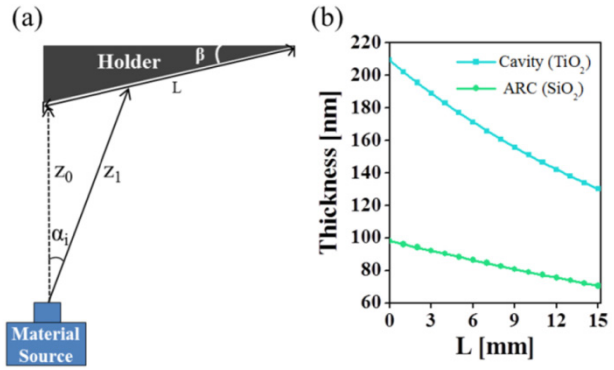

Fig. 6. (a) Schematic diagram of the proposed glancing angle deposition. (b) Calculated thicknesses of the cavity and ARC as a function of position along the substrate.

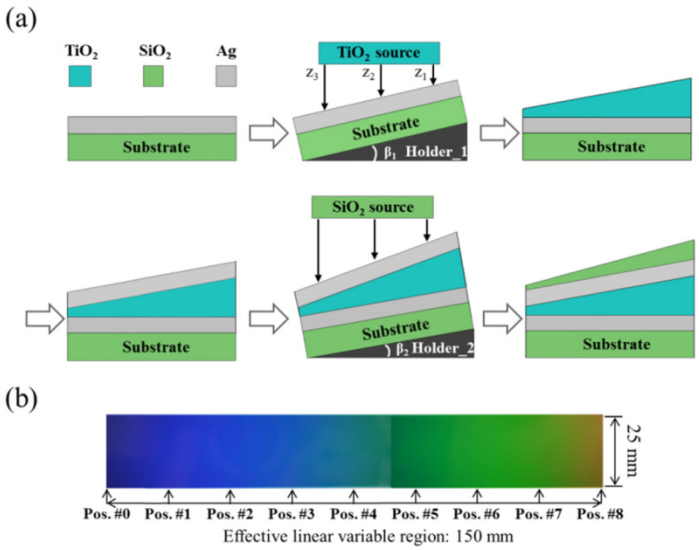

Fig. 7. (a) Fabrication procedure for the proposed LVCF. (b) Color images for the fabricated device.

For the fabricated LVCF, as specified in Fig. 2, the transfer characteristics with respect to the position were inspected using a spectrometer (USB4000, Ocean Optics) for normally incident unpolarized light. Considering the position-dependent characteristics of the LVCF,

Optics EXPRESS

the spot size of the light beam impinging upon the device was minimized down to as small as 500 μm in diameter with the help of a pinhole. As shown in Fig. 8(a), the center wavelength ranged from 410 nm to 566 nm as the observation point moves from Pos. #0 to Pos. #8 along the sample, leading to an effective LFR of 156 nm. Accordingly, the spectral bandwidth and peak transmission were about 68 nm and 40% on average, respectively, which are about 33 nm broader and 20% lower compared to the results of the calculation. The observed spectra might be susceptible to scattering incurred by the rough surface of the deposited Ag layer. An Ag film deposited on a dielectric substrate was reported to provide a discrete granular morphology with random metal-island growth [32–34], and the scattering induced loss may be efficiently alleviated by smoothing the surface of the Ag film by taking advantage of a wetting layer, such as that made from germanium (Ge) or a polymer [32–34]. For instance, an ultra-thin polymer in PTCBI or PEI can be coated beneath the Ag film so as to prevent the random migration and aggregation of the deposited Ag atoms [33,34]. Figure 8(b) plots the resonance wavelength as a function of the position. It was concretely indicated that a linear relationship between the resonance wavelength and the position was obtained both for the calculation and the measurement results, exhibiting a linearity beyond 99% according to the least squares method [35].

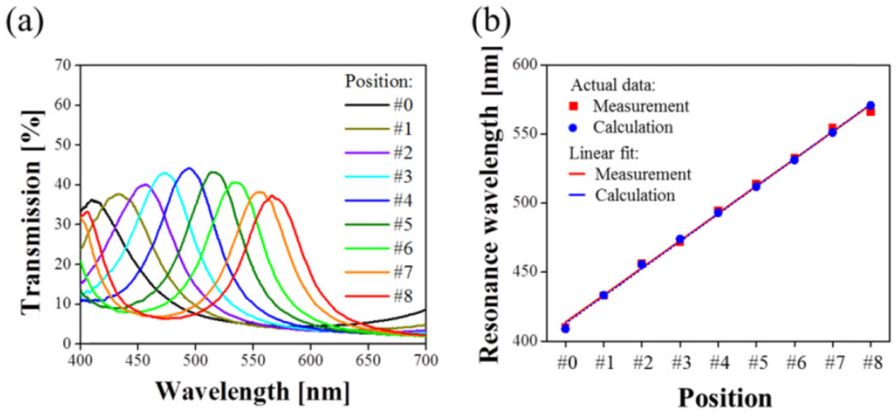

Fig. 8. (a) Measured transmission spectra and (b) resonance wavelength with the position along the LVCF.

Figure 9 shows the measured transmission spectra as a function of the incident angle monitored for Pos. #1, Pos. #4, and Pos. #7, which resonantly peaked at λ = 433 nm, 495 nm, and 554 nm, respectively. For the incident angle of 45°, the corresponding spectral shifts were $\Delta\lambda$ = 18.3 nm, 18.2 nm, and 21.2 nm, respectively, which approximately translate into fractional wavelength shifts of $\Delta\lambda/\lambda$ = 4.2%, 3.7%, and 3.8%. The resulting degradation in the peak transmission was about 14% on average over the angular range. As predicted from the results of the calculation given in Fig. 4, the proposed LVCF was practically corroborated to have a spectral response that is substantially tolerant to an incident angle ranging up to 45°, which is primarily beneficial for its applications in spectrometer and hyperspectral imaging.

Optics EXPRESS

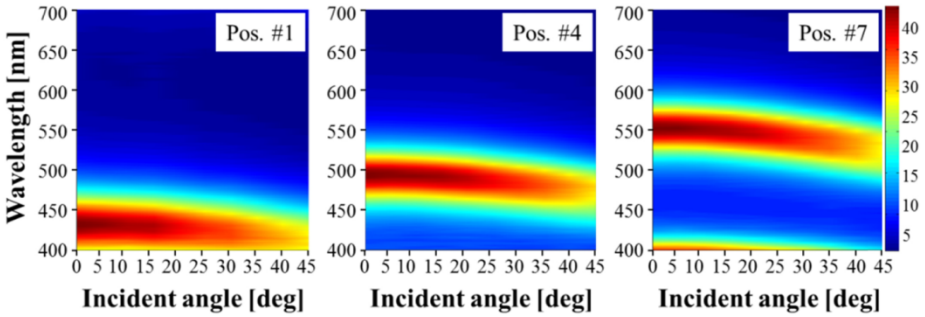

Fig. 9. Measured transmission spectra with the incident angle for different positions.

4. Conclusion

An LVCF was embodied by resorting to an etalon with an Ag-TiO_2-Ag configuration that is integrated with a tapered ARC in SiO_2. Glancing angle deposition was applied in a straightforward process to pertinently taper the dielectric cavity so that the resonance wavelength can be continuously scanned according to the position, and the ARC was tapered to adaptively elevate the transmission across the entire device. As intended, the LFR was observed to be 156 nm, ranging from 410 nm to 566 nm, and the angle-insensitive resonance was stable under oblique incidences running up to 45°. The resonance wavelength was experimentally verified to be linearly dependent on the position, leading to a linearity beyond 99%. When compared to conventional all-dielectric LVCFs based on Bragg reflectors, the proposed LVCF could enable a relaxed angular tolerance, an enlarged LFR, and facile fabrication while providing a relatively low transmission and wide bandwidth.

Appendix A: Material properties

The refractive indices of Ag and $Ti0_2$ adopted for simulation are shown below, in Fig. 10.

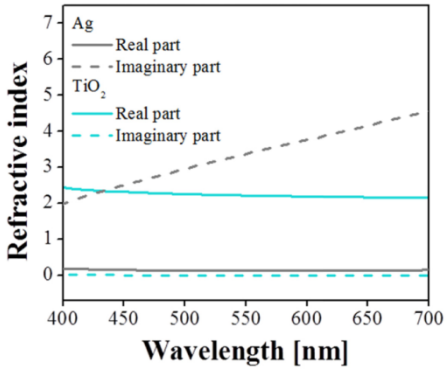

Fig. 10. Refractive indices of Ag and TiO_2 adopted for simulation.

Funding

National Research Foundation of Korea (NRF) grant funded by the Korean government (MSIP) (No. 2016R1A2B2010170); ARC Future Fellowship FT110100853.